ISSN 1330-3651 (Print), ISSN 1848-6339 (Online) https://doi.org/10.17559/TV-20230918000945
Original scientific paper

Neural Network-Based Optimization of the Electrical Discharge Drilling Process Parameters

An-Le VAN, Trung-Thanh NGUYEN, Phan NGUYEN HUU, Xuan-Ba DANG*

Abstract: The current work aims to optimize process parameters, including the current (*I*), voltage (*V*), pulse on time (*O*), and pulse off time (*F*) of the electrical discharge drilling of the small hole (EDDH) to reduce the dilation of the drilled hole (*DH*) as well as the tapper of the drilled hole (*HT*) and enhance the material removal rate (*MRR*). The radial basis function network (RBFN) was used to develop EDDH responses, while the modified quantum-behaved particle swarm optimization algorithm (MQPSO) was applied to produce feasible solutions. The evaluation by an area-based method of ranking (EAMR) approach was used to select the best optimality. The obtained results indicated that the optimal *I*, *V*, *O*, and *F* are 5 A, 60 V, 40 µs, and 45 µs, respectively. The *DH* and *TP* are reduced by 32.8% and 28.0%, while the *MRR* is improved by 66.3%. The RBFN models could be effectively applied to present non-linear data. The *DH* and *TP* models were significantly affected by the *O* and *F*, while the *I* and *V* had effective influences on the *MRR*. The outcomes could be used to improve the drilled quality indicator and productivity in industrial EDDH applications.

Keywords: dilation; electrical drilling; process parameters; removal rate; tapper

1 INTRODUCTION

The EDDH is frequently used to create tiny holes for various materials. High discharge energy is used to melt and evaporate the material, and a dielectric fluid is used to remove any leftover debris. Zero machining force and non-contact between the specimen and electrode allow for the fabrication of small dimensions. Notable benefits include low tolerance, high machined part accuracy, zero mechanical stress, machining higher-hardness material, and flexibility.

Performance metrics have been improved by taking into account and optimizing various EDDH activities. The *DH*, *TP*, drilled circularity (*DC*), material removal rate (*MRR*), tool wear rate (*TWR*), surface roughness (*SR*), and micro-hardness (*MH*) are the conventional answers. Using the ANFIS model and genetic algorithm, the *I*, *O*, *F*, and electrode diameters of the EDDH Inconel 825 were tuned to improve the *MRR*, *HC*, and *TP* [1]. The results showed that the suggested method greatly improved the EDD process's machining performance. In terms of the *I*, *O*, *F*, tool rotation, and vibration amplitude, the empirical models of the *MRR* and *SR* of the EDDH titanium alloy were created [2]. The outcomes showed that, with prediction errors of less than 9%, the proposed mathematical models for *MRR* and *SR* accurately represented the experimental data. For the EDDH metal matrix composite, Davis et al. highlighted that the hollow cylindrical tool electrode could obtain 33.79% greater MRR as compared to the solid conical tool electrode [3]. According to Naik et al., the *I* made a large contribution to the EDDH Al-SiC metal matrix composite (72.23% for *MRR*, 40.56% for *SR*, and 34.01% for *MH*) [4]. An analysis was done on the effects of the V and tool rotation on the *DC*, *MRR*, and *TWR* of the EDDH nickel-titanium [5]. The *V* was shown to be the important determining element for increasing the pace of machining, according to the results. According to Gao et al., to minimize surface flaws in the EDDH nickel-based superalloy, lower *I*, *O*, and higher *F* values were advised [6]. For the EDDH titanium, the effects of the *V*, capacitance, and feed rate on the *MRR*, *TWR*, *DC*, and *TP* were examined [7]. In comparison to feed rate, the results showed that capacitance and *V* were the most important variables for all response metrics. According to Saxena et al., utilizing the ideal *V* and workpiece thickness improved the *MRR* and *TWR* of the EDDH N-BK7 glass by 25% and 7%, respectively [8]. A new dielectric fluid based on copper powder was created to improve the EDDHTi-6Al-4V metallic output parameters [9]. According to the results, the *MRR* was 33% higher than the conventional one. To increase the *MH* and lower the *SR*, the ideal *I*, *O*, and *V* of the EDDH superalloy superfer 800 were chosen [10]. The findings showed that the *SR* and *MH* had improved by 52% and 61%, respectively. For the EDDH AZ91composite, the *MRR* and *SR* artificial neural network models were created [11]. The results showed that at optimality, the *MRR* was increased by 26.5% and the *SR* was decreased by 15.8%. Gunasekar et al. reported that neem oil was used to increase the 67.5% *MRR*, 26% *TWR*, and 24% *SR* for the EDDH AA8011 composite [12]. According to Pratap et al., tungsten carbide produced the lowest *SR*, whereas copper electrodes caused the highest *MRR* [13]. Pandey and Yadav highlighted that with vibration assistance, the *MRR* of the EDDH Al-TiB2 could be raised by 36.8% [14]. The development of the cryogenic EDDH resulted in a 62% and 36% increase in *MRR* and *SR*, respectively, as well as an improvement in productivity and surface quality [15]. However, the shortcomings of related publications can be expressed as:

The influences of the *I*, *V*, *O*, and *F* on the *DH*, *TP*, and *MRR* for the drilled hole of the stainless steel have not been presented. The *DH*, *TP*, and *MRR* models for the EDDH stainless steel operation have not been developed. Moreover, the optimal EDDH stainless steel process parameters have not been selected to boost the quality and productivity indicators.

The objective of this work is to optimize four key process parameters of the EDDH stainless steel operation for minimizing dilation as well as the tapper of the drilled hole and improving the *MRR*.

In the current work, the radial basis function network is proposed to present non-linear data on performance measures instead of conventional RSM models. Moreover, an efficient algorithm entitled the modified quantum-behaved particle swarm optimization algorithm is applied to find optimal solutions.

The scientific contributions are expressed as:

The optimizing findings of EDDH factors and output objectives can be applied to practical EDDH operations to enhance quality indicators and productivity.

The technological understanding of the EDDH process can be greatly enhanced by utilizing the effects of EDDH elements on the output objectives.

The RBFN-MQPSO-EAMR can be applied to treat optimizing issues in not only the EDDH operation but also different machining operations. The experimental costs, human effort, and machining time can be saved with the support of the developed method.

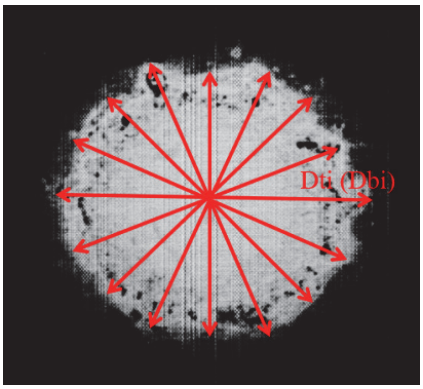

(a) For computing D_T or D_B

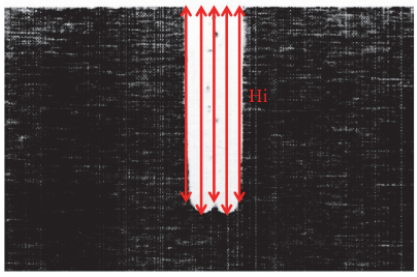

(b) For computing H

Figure 1 The scheme of the diameters and drilled depth

2 OPTIMIZING METHOD

The DH (mm) value is computed as:

$$DH = \frac{D_T - D_O}{2} \tag{1}$$

where D_T and D_O are the average top diameter and the original tool's diameter, respectively.

The D_T is computed as (Fig. 1a):

$$D_T = \frac{\sum_{1}^{n} D_{ti}}{n} \tag{2}$$

where D_{ti} is the top diameter at the i_{th} position.

The TP value is computed as:

$$TP = \frac{D_T - D_B}{2 \times H} \tag{3}$$

where D_B and H present the average bottom diameter and drilled depth, respectively. The D_B is computed as:

$$D_B = \frac{\sum_{1}^{n} D_{bi}}{n} \tag{4}$$

where D_{bi} is the bottom diameter at the i_{th} position.

The H is computed as (Fig. 1b):

$$H = \frac{\sum_{1}^{n} H_i}{n} \tag{5}$$

where H_i is the drilled depth at the i_{th} position.

The MRR (mm^3/s) is computed as:

$$MRR = \frac{\Pi (D_T + D_B)^2 H}{16t} \tag{6}$$

where t(s) is the drilling time.

The EDDH factors, including the I, V, O, and F are listed as optimization parameters (Tab. 1). The current, voltage, pulse on time, and pulse off time are key factors that have significant impacts on the quality criteria and production rate. Their values are chosen based on the manual book and the characteristics of the EDD machine. Additionally, parameter ranges are selected according to the recommendations of the electrode's manufacturer. These ranges are verified by the aforementioned works and mechanical experts. The optimizing problem is presented as:

Find $X = (I, V, O, \text{and } F)$

Reducing DH and TP; Enhancing MRR

Conditions: $2 \le I \le 8$ A; $40 \le V \le 60$ V; $40 \le O \le 90$ µs; $30 \le F \le 60$ µs.

Table 1 Process inputs for the SPRT process

Symbol	Parameters	Values
I	Discharge current / A	2-5-8
V	Discharge voltage / V	40-50-60
O	Pulse on time / µs	40-65-90
V	Pulse off time / µs	30-45-60

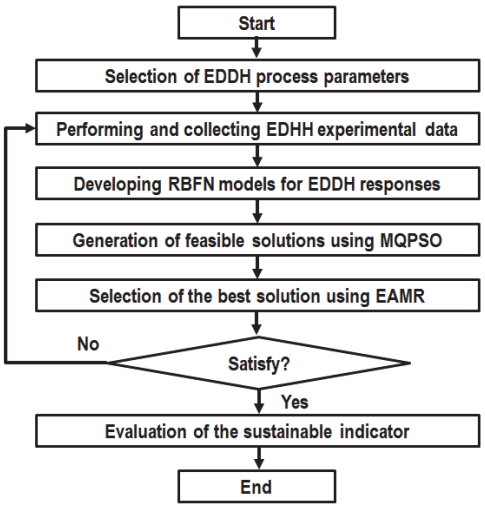

Figure 2 Optimization approach for the EDDH operation

The optimizing procedure for the EDDH process is illustrated in Fig. 2:

Step 1: Executing EDDH experiments using the Box-Behnken design [16, 17].

The Box-Behnken approach uses the lowest, middle, and maximum ranges for each factor (–1, 0 +1). The block's edge and center are designated as the design points. This method reduces the quantity of trials, which lowers expenses and labor requirements. In the Box-Behnken approach, the number of experiments (N) is computed as follows:

$$N = 2m(m-1) + P_c \tag{7}$$

where the m and P_c stand for the number of parameters and center points, respectively. 29 experiments are produced in this study because four process parameters with three levels and five center points are used.

Step 2: The EDDH responses are developed using the RBFN approach.

The RBFN using the Gaussian function is used to present the correlations between the inputs and outputs [18]. The input parameters are combined into the hidden one, while the output for the given input (s) and vector (c_i) is expressed as:

$$out_i = \exp(-\frac{1}{2\sigma^2}\|s - c_i\|^2) \tag{8}$$

where $\|s - c_i\|$ is the Euclidean distance between s and c_i.

The Gaussian function is expressed as:

$$\Phi(r) = \exp(-\gamma r^2) \tag{9}$$

where γ is a parameter, which is found using the cross-validation stage.

The RBFN model for a given input s is expressed as:

$$out = w_0 + \sum_{i=1}^{m} w_i \exp(-\frac{1}{2\sigma^2}\|s - c_i\|^2) \tag{10}$$

where w_0 and w_m are the bias and weight assigned to the hidden output, respectively. To minimize the predictive deviation, the assigned weight is computed as:

$$w = (H^T H)^{-1} H^T r \tag{11}$$

where r presents the response vector. H is the design matrix and is expressed as:

$$H(j,i) = \exp(-\frac{1}{2\sigma^2}\|s - c_i\|^2) \tag{12}$$

Step 3: Generation of feasible solutions using the MQPSO.

PSO is the foundation of the QPSO algorithm. The quantum model of particles is used to propose the QPSO algorithm. A particle in quantum space cannot have its position and speed precisely known; instead, a wave function must determine its position. Using the Monte Carlo stochastic simulation technique, the particle's position is given by:

$$x_{i,j}(t+1) = p_{i,j}(t) \\ -\alpha\left|c_j(t) - x_{i,j}(t)\right| \times \ln(\frac{1}{u_{i,j}(t)}) \tag{13}$$

$$p_{i,j}(t) = \beta p_{besti,j} + (1-\beta) gbest_j \tag{14}$$

where random values from 0 to 1 that fulfill uniform distribution are represented by $u_{i,j}(t)$ and β. The j_{th} dimension of the particle's ideal location is denoted by $gbest_j$. The j_{th} dimension of particle 's optimum position is denoted by $pbest_{i,j}$. QPSO has only one parameter, α, which is the expansion-contraction factor. As of right now, the most popular approach involves linearly reducing the value of α from 0.9 to 0.4, where $c_j(t)$ is the average of all the particles' ideal positions during this iteration.

Because QPSO can create greater perturbations, we altered it with a Cauchy-Lorentz distribution (CD). During the mutation stage, a new position (x') is expressed as:

$$x' = x + \lambda R \tag{15}$$

where R is the random value mutation at x location.

The following is the selection technique approach for N particles:

$$f(x(t)) = \{f(x_1(t)), ...f(x_N(t))\} \tag{16}$$

where the swarm's fitness function and particle location vector are denoted by $f(x(t))$ and $x(t)$, respectively. The modified positions of the swarm particles in the subsequent iteration are shown as follows:

$$x'(t) = \{x_1''(t), ...x_a''(t)\} \\ x''_k(t) = \{x_1'(t), ..x_b'(t)\} \tag{17}$$

where a and b stand for the number of best places and the selection parameter, respectively.

The operation of the MQPSO is presented in Fig. 3.

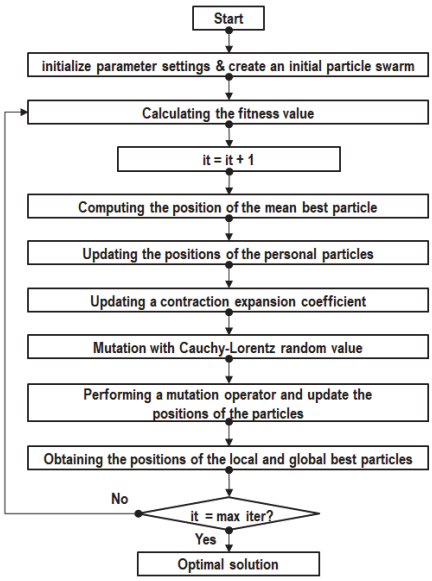

Figure 3 The working principle of the MQPSO

Step 4: The EAMR method is utilized to select the best optimal point.

The normalized response (n_{ij}) is calculated as:

$$n_{ij} = \frac{y_{ij}}{\max y_{ij}} \tag{18}$$

The weighted response (v_{ij}) is computed as:

$$v_{ij} = \omega_j(n_{ij}) \tag{19}$$

The normalized point for the criteria is computed as:

$$G_i^+ = v_{i1}^+ + v_{i2}^+ + ...v_{im}^+ \quad \text{For the higher aim} \tag{20}$$

$$G_i^+ = v_{i1}^+ + v_{i2}^+ + ...v_{im}^+ \quad \text{For the smaller aim} \tag{21}$$

The performance indicator (I_i) is computed as:

$$I_i = \frac{G_i^+}{G_i^-} \tag{22}$$

The highest I_i is the best solution.

Table 2 Chemical compositions of the SS 304H

Elements	C	Si	Mn	P	S	Cr	Ni	N	Fe
%	0.04	0.75	2.00	0.045	0.03	19.12	9.50	0.10	Balance

3 EXPERIMENTAL SETTING

A CNC EDM machine is used for the EDDH trials (Fig. 4). To remove the substance, the electrode is continuously rotated and moved. The dimensions are 1.2 mm for the outer diameter and 0.6 mm for the inner one. The machined table has the specimen tightly gripped on it. Each specimen measures 30 mm in length, 16 mm in width, and 14 mm in height. The workpiece is made of a higher-carbon-content stainless steel called SS304H, which finds considerable use in heat exchangers, pressure vessels, and the power generation sector. Tab. 2 displays the chemical components of the SS304H.

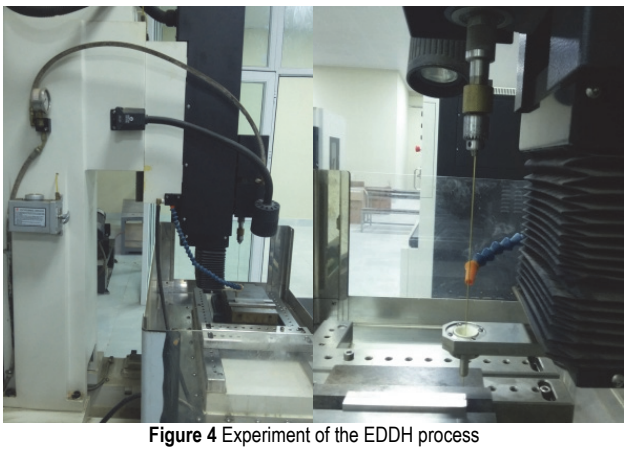

Figure 4 Experiment of the EDDH process

At a low V, low intensity of discharge energy is used to remove the material, leading to a uniform distribution of the top diameter (Fig. 5a). A higher V causes an increase in discharge energy, and more effective sparking is generated to enlarge the top diameter (Fig. 5b). A low discharge energy is produced at a low V, leading to a shallow depth (Fig. 5c). A higher drilled depth is produced with an increased V due to an increment in discharge energy (Fig. 5d). At a low V, low intensity of discharge energy generates a smooth surface without any defects. Small cracks, little voids, and small holes are produced (Fig. 5e). A higher V causes excessive discharge energy, and the machined surface is affected by more effective sparking. The surface defects, including the larger cracks, bigger voids, and larger holes are produced (Fig. 5f).

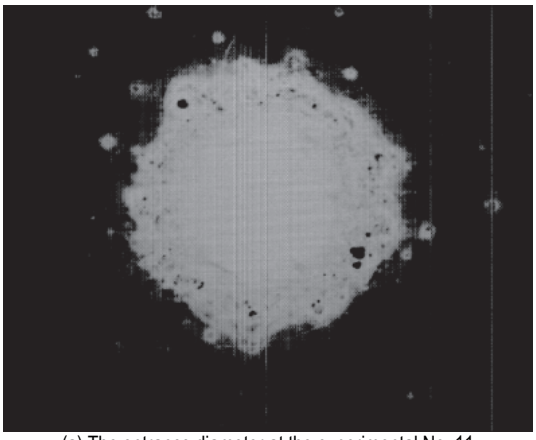

(a) The entrance diameter at the experimental No. 11

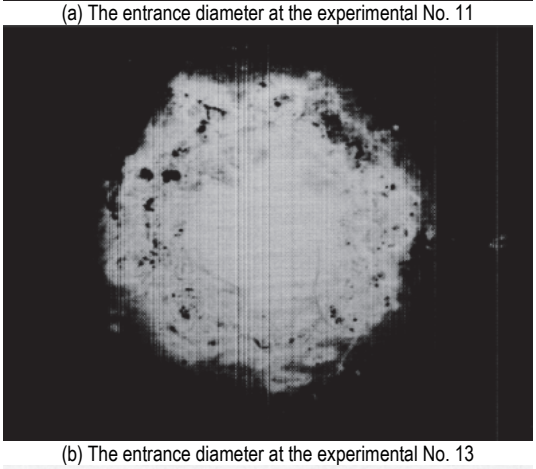

(b) The entrance diameter at the experimental No. 13

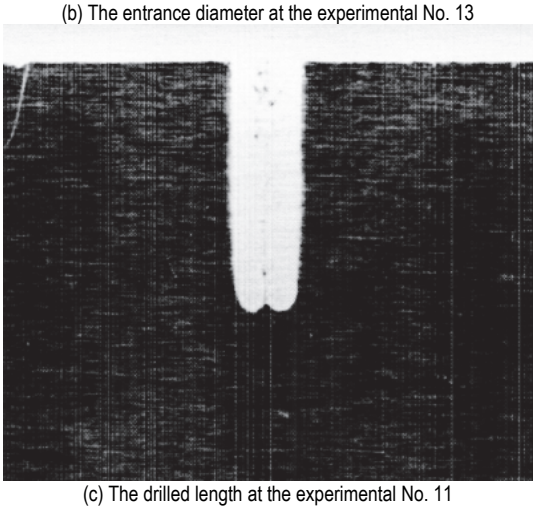

(c) The drilled length at the experimental No. 11

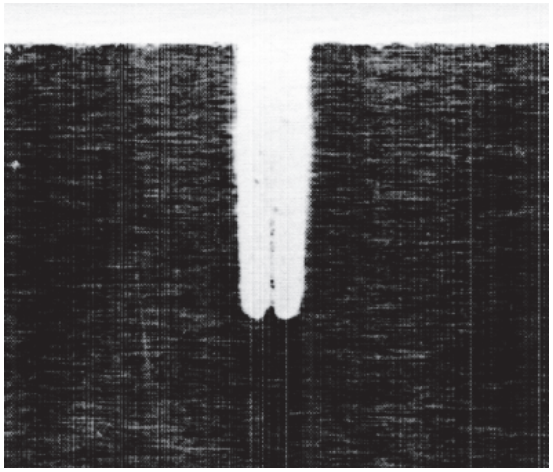

(d) The drilled length at the experimental No. 13

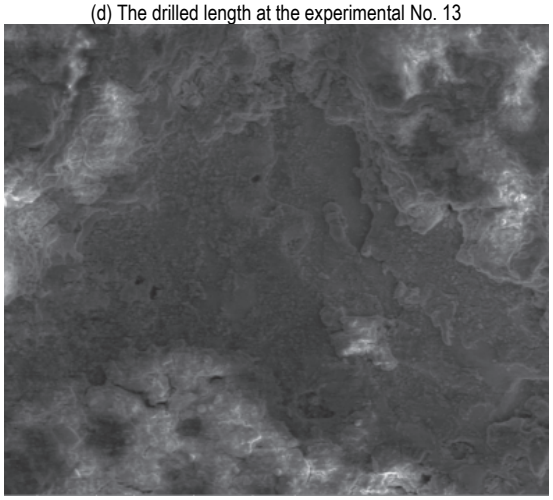

(e) The drilled surface at the experimental No. 11

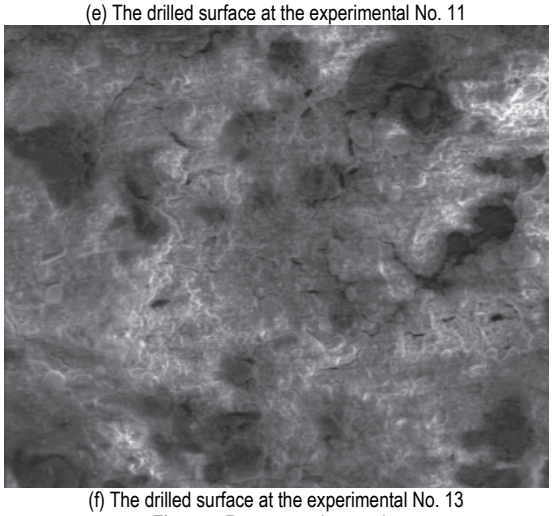

(f) The drilled surface at the experimental No. 13

Figure 5 Representative results

4 RESULTS AND DISCUSSIONS

4.1 Parametric Influences

The experimental outcomes for the EDDH operation are presented in Tab. 3.

Table 3 Experimental data for the EDDH process

No.	*I* / A	*V* / V	*O* / μs	*F* / μs	*DH* / μm	*TP* × 10^{-3}	*MRR* / mm^3/s
Experimental data for optimizing and developing predictive models							
1	2	50	65	30	406	30.1	0.5819
2	5	50	65	45	427	30.7	0.8723
3	8	50	65	60	304	25.7	0.7613
4	5	60	65	30	408	24.5	1.2465
5	2	50	90	45	414	34.1	1.0546
6	5	50	40	30	386	30.5	0.9367
7	5	50	65	45	426	30.4	0.8778
8	5	50	40	60	310	26.2	0.6505
9	2	40	65	45	322	26.1	0.4789
10	5	50	90	30	476	36.9	1.3765
11	5	40	65	30	389	32.9	1.0066
12	8	50	40	45	343	26.9	0.9954
13	2	60	65	45	311	23.7	0.8742
14	5	40	40	45	286	26.4	0.4306
15	8	60	65	45	316	22.2	1.4489
16	5	50	65	45	427	30.3	0.8788
17	5	60	40	45	304	24.3	1.0006
18	5	50	90	60	372	32.1	1.0015
19	5	60	65	60	308	26.1	1.1482
20	2	50	65	60	338	25.9	0.8151
21	8	50	90	45	392	31.1	1.297
22	5	40	90	45	396	33.8	1.1041
23	2	50	40	45	302	25.4	0.3698
24	5	50	65	45	428	31	0.8793
25	5	60	90	45	361	30.1	1.2573
26	8	40	65	45	313	26.3	0.7938
27	8	50	65	30	433	28.9	1.6767
28	5	40	65	60	307	23.1	0.4188
29	5	50	65	45	424	30.7	0.8731
Experimental data for testing models							
30	3	45	50	35	363	29.6	0.4957
31	4	55	60	55	362	27.6	0.8926
32	6	48	70	50	407	30.1	0.8624
33	7	42	80	40	398	32.1	1.1578
34	3	52	85	45	426	33.3	1.0087
35	6	58	55	55	327	26.1	1.0538

Table 4 Computed ANOVA results for the *DH*

So.	SS	MS	F value	p-value
Model	80892.0	5778.0	42.1	< 0.0001
I	5.3	5.3	0.038	0.7239
V	2.1	2.1	0.015	0.825
O	19200.0	19200.0	136.364	< 0.0001
F	26040.1	26040.1	184.944	< 0.0001
IV	49.0	49.0	0.348	0.2931
IO	992.3	992.3	7.047	0.0002
IF	930.2	930.3	6.607	0.0003
VO	702.2	702.3	4.988	0.5232
VF	81.0	81.0	0.575	0.1819
OF	196.0	196.0	1.392	0.4642
I^2	11988.9	11988.9	85.148	< 0.0001
V^2	27083.1	27083.1	192.352	< 0.0001
O^2	3890.9	3890.9	27.634	< 0.0001
F^2	1032.5	1032.5	7.333	0.0002
Res.	1921.3	137.2		
Cor.	82813.2			
R^2: 0.9768; Adj. R^2: 0.9602; Pred. R^2: 0.9526				

The *DH* has two contradictory trends when the *I* changes (Fig. 6a). A higher *I* increases the amount of discharge energy transferred to the workpiece. More effective sparking is produced to melt and evaporate material. Higher values of the top and bottom diameters are produced; hence, a higher *DH* is generated. As the *I* changes from 5 to 8 A, excessive discharging energy decreases the diameter of the electrode due to higher erosion. Lower top and bottom diameters are produced; hence, the *DH* reduces.

The *DH* has two contradictory trends when the *V* changes (Fig. 6b). A higher *V* increases discharge energy transferred to the specimen. More effective sparking is produced to evaporate material. Higher top and bottom diameters are generated; hence, a higher *DH* is produced. A further *V* causes excessive discharging energy, leading to a higher erosion of the tool. Lower top and bottom diameters are generated; hence, the *DH* decreases.

The *DH* has a relative increment when the *O* changes (Fig. 6c). A higher *O* increases the discharging time and more effective sparking is used to melt and evaporate material. Higher values of the top and bottom diameters are produced, leading to an increase in the *DH*. A further *O* increases the erosion of the electrode, leading to a reduction in the tool's diameter. Lower top and bottom diameters are produced; hence, the *DH* decreases.

The *DH* has a relative reduction when the *F* changes (Fig. 6d). A higher *F* decreases the intensity of discharge energy due to low processing time. The low degree of material evaporation is produced. Lower top and bottom diameters are produced; hence, the *DH* decreases.

ANOVA results are used to investigate the model's significance and parameter contributions. The level of significance is 0.05, which is a confidence level of 95%. The factors with a p-value less than 0.05 are listed as significant terms.

The analyzed percentages of EDDH factors for the *DH* are presented in Tab. 4. We find that "F value" of the model is 42.1, which confirms that it is significant. R^2 of 0.9768 is in reasonable agreement with the adjust R^2 of 0.9602. The predicted R^2 = 0.9526 and adjust R^2 = 0.9602 have almost the same values; the deviation is less than 0.2. Therefore, the *DH* model is considered adequate and can accurately predict the response in the range of EDDH conditions used. Computed percentages of the *O* and *F* are 20.83% and 28.24%, respectively. Computed percentages of the *IO* and *IF* are 1.08% and 1.01%, respectively. Computed percentages of the I^2, V^2, O^2, and F^2 are 13.0%, 29.38%%, 4.22%, and 1.12%, respectively.

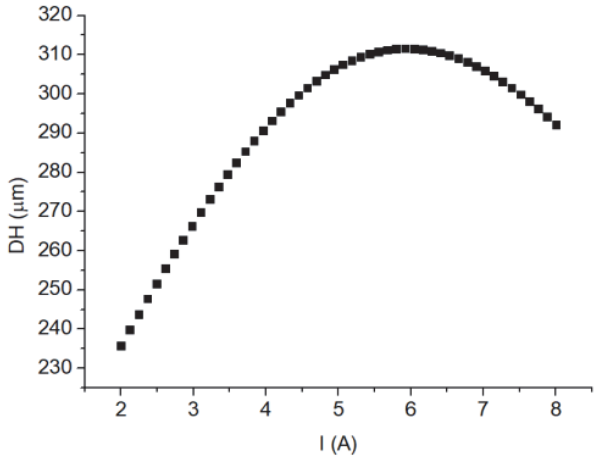

(a) *DH* versus *I*

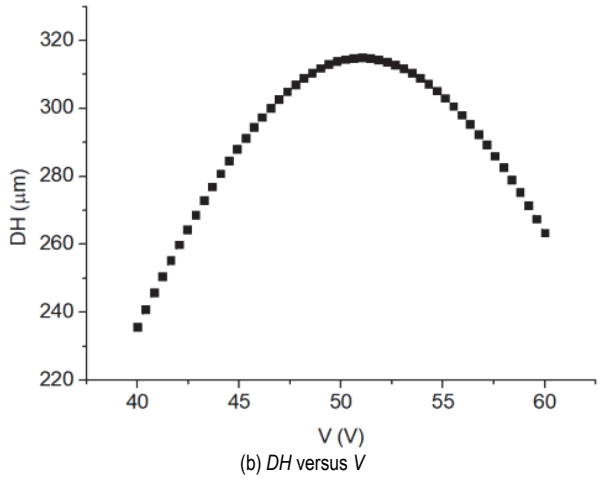

(b) *DH* versus *V*

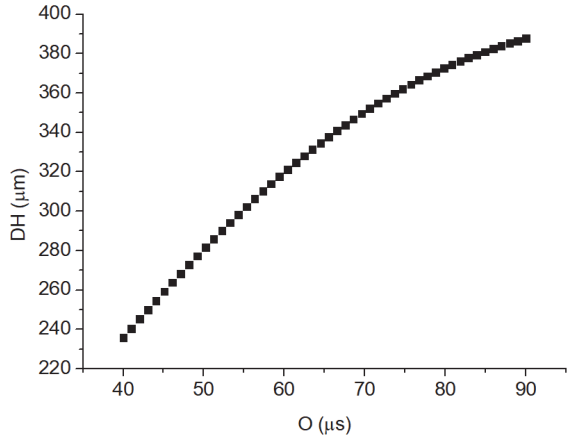

(c) *DH* versus *O*

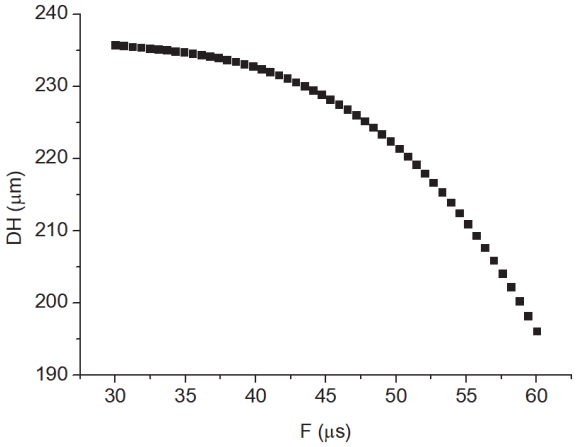

(d) *DH* versus *F*

Figure 6 The impacts of EDDH parameters on the DH

The *TP* has two contradictory trends when the *I* changes (Fig. 7a). A higher *I* increases discharge energy, which is used to enlarge top and bottom diameters. More material is removed and the *TP* increases. The tool length decreases with an increased *I* due to excessive discharge energy, leading to ineffective sparking; hence, the *TP* decreases.

The *TP* has two contradictory trends when the *V* changes (Fig. 7b). An increased *V* enhances discharge energy, leading to a higher degree of material evaporation. The top and bottom diameters enlarge; hence, the *TP* increases. A further *V* causes excessive discharge energy, leading to a reduced tool's length and diameter. Lower values of the drilled diameters and depths are produced; hence, the *TP* decreases.

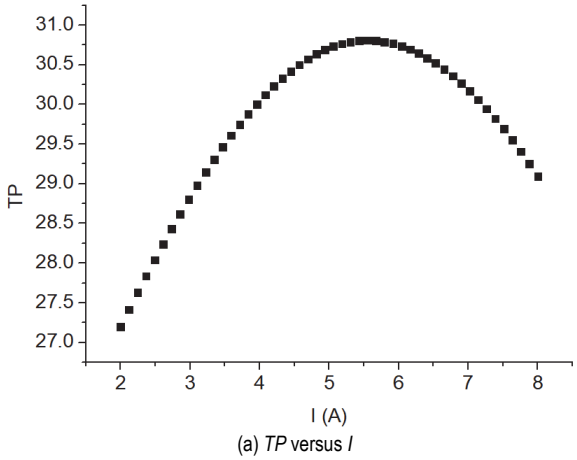

(a) *TP* versus *I*

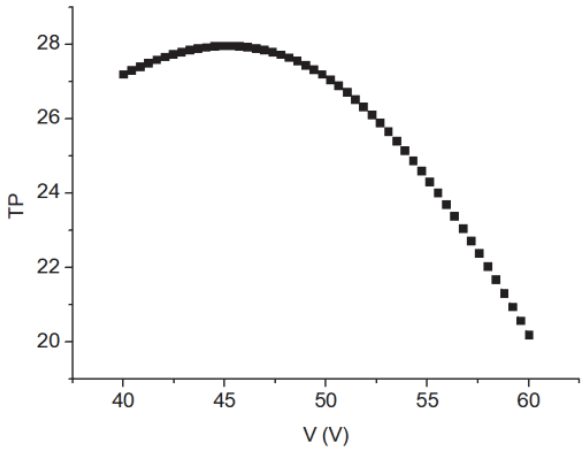

(b) *TP* versus *V*

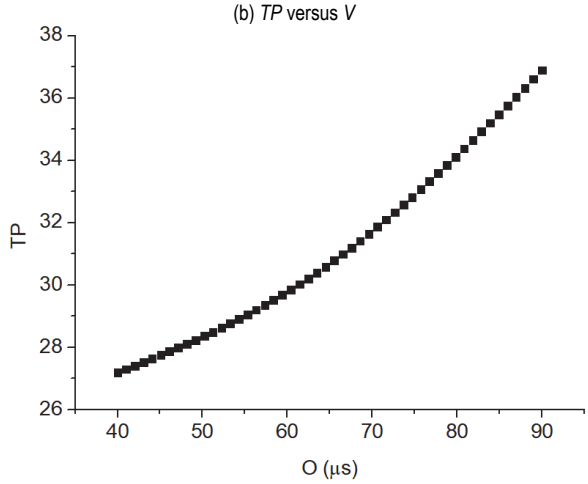

(c) *TP* versus *O*

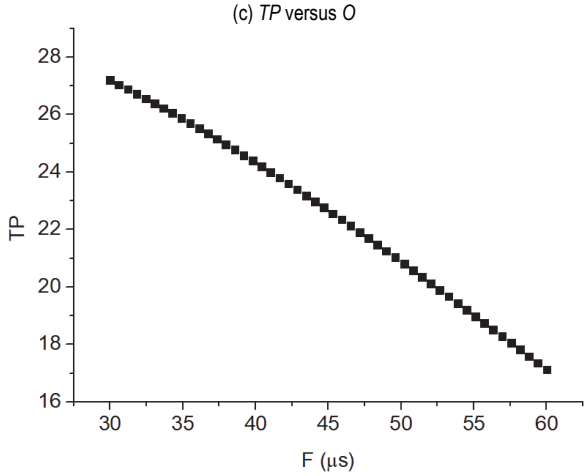

(d) *TP* versus *F*

Figure 7 The impacts of EDDH parameters on the TP

The *TP* increases when the *O* changes (Fig. 7c). A higher *O* increases the processing time between the electrode and material, leading to effective sparking. More energy is produced to remove the material, leading to increments in the drilled diameters and lengths; hence, the *TP* increases.

The *TP* decreases when the *F* increases (Fig. 7d). A higher *F* decreases the processing time between the electrode and material, leading to a reduction in discharge energy. Lower values of the drilled diamters and depths are produced; hence, the *TP* reduces.

Analyzed percentages of EDDH factors for the *TP* are presented in Tab. 5. We find that "F value" of the model is 49.54, which confirms that it is significant. R^2 of 0.9813 is in reasonable agreement with the adjust R^2 of 0.9642. The predicted R^2 = 0.9501 and adjust R^2 = 0.9642 have almost the same values; the deviation is less than 0.2. Therefore, the *TP* model is considered adequate and can accurately predict the response in the range of EDDH conditions used. Computed percentages of the *V*, *O*, and *F* are 7.00%, 32.95%, and 13.63%, respectively. Computed percentages of the *IO* and *VF* are 1.36% and 8.71%, respectively. Computed percentages of the I^2, V^2, and O^2 are 11.44%, 20.42%, and 3.22%, respectively.

Table 5 Computed ANOVA results for the *TP*

So.	SS	MS	F value	p-value
Model	372.41	26.60	49.54	< 0.0001
I	1.47	1.47	2.74	0.8642
V	26.11	26.11	48.62	< 0.0001
O	122.88	122.88	228.83	< 0.0001
F	50.84	50.84	94.67	< 0.0001
IV	0.72	0.72	1.34	0.3762
IO	5.06	5.06	9.42	< 0.0001
IF	0.25	0.25	0.47	0.8632
VO	0.64	0.64	1.19	0.3642
VF	32.49	32.49	60.50	< 0.0001
OF	0.06	0.06	0.12	0.9264
I^2	42.65	42.65	79.42	< 0.0001
V^2	76.16	76.16	141.82	< 0.0001
O^2	12.01	12.01	22.36	< 0.0001
F^2	1.63	1.63	3.04	0.8569
Res.	7.10	0.51		
Cor.	379.51			
R^2: 0.9813; Adj. R^2: 0.9642; Pred. R^2: 0.9501				

The *MRR* increases when the *I* changes (Fig. 8a). A higher *I* increases discharge energy to remove the material. More effective sparking is used to increase the drilled diameters and depths; hence, the *MRR* increases.

The *MRR* is enhanced when the *V* increases (Fig. 8b). A higher *V* increases discharge energy, which enhances the drilled diameters and lengths. A higher degree of material removal is produced; hence, the *MRR* enhances.

The *MRR* is improved when the *O* changes (Fig. 8c). A higher *O* increases the processing time between the electrode and specimen. More effective sparking is used to increase the drilled diameters and depths; hence, the *MRR* is enhanced.

The *MRR* is reduced when the *F* changes (Fig. 8d). A higher *F* reduces the processing time between the electrode and specimen. The intensity of the discharge energy decreases, leading to lower drilled diameters and depths; hence, the *MRR* decreases.

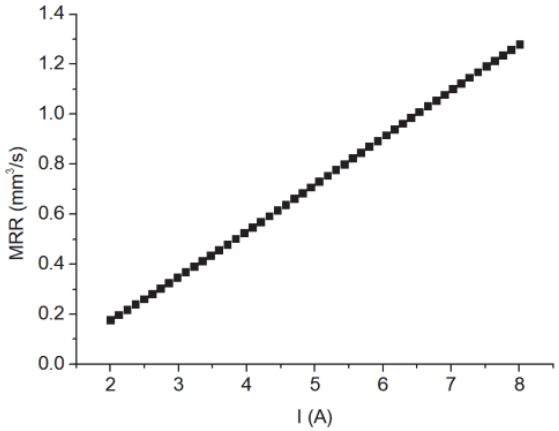

(a) *MRR* versus *I*

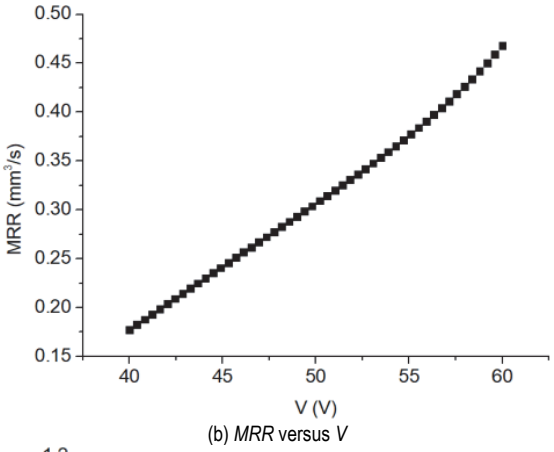

(b) *MRR* versus *V*

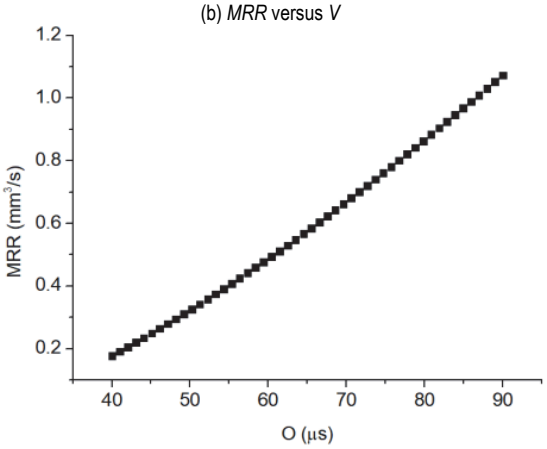

(c) *MRR* versus *O*

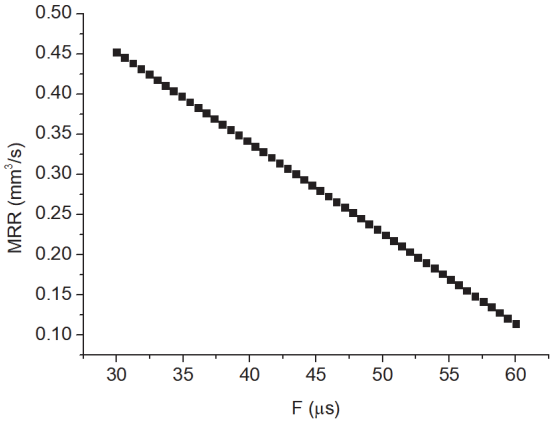

(d) *MRR* versus *F*

Figure 8 The impacts of EDDH parameters on the MRR

ANOVA results for the *MRR* are presented in Table 6. We find that "F value" of the model is 48.735, which confirms that it is significant. R^2 of 0.9768 is in reasonable agreement with the adjust R^2 of 0.9626. The predicted R^2 = 0.9538 and adjust R^2 = 0.9626 have almost the same values; the deviation is less than 0.2. Therefore, the *MRR* model is considered adequate and can accurately predict the response in the range of EDDH conditions used. Computed percentages of the *I*, *V*, *O*, and *F* are 23.49%, 22.77%, 22.04%, and 12.29%, respectively (Fig. 13). Computed percentages of the *IO*, *IF*, *VO*, and *VF* are 1.34%, 11.93%, 1.55%, and 2.17%, respectively. Computed percentage of the F^2 is 1.08%, respectively.

Table 7 Comparisons between the experimental and predictive values for the RBFI models

No.	*DH* / µm		Err.	*TP*		Err.	*MRR* / mm³/s		Err.
30	363	358	1.38	29.6	28.9	2.36	0.4957	0.4968	–0.22
31	362	372	–2.76	27.6	28.2	–2.17	0.8926	0.8948	–0.25
32	407	415	–1.97	30.1	30.7	–1.99	0.8624	0.8656	–0.37
33	398	408	–2.51	32.1	31.8	0.93	1.1578	1.1592	–0.12
34	426	435	–2.11	33.3	33.8	–1.50	1.0087	1.0046	0.41
35	327	336	–2.75	26.1	26.8	–2.68	1.0538	1.0582	–0.42

Table 8 Optimization outcomes

Method	*I* / A	*V* / V	*O* / µs	*F* / µs	*DH* / µm	*TP* / ×10⁻³)	*MRR* / mm³/s	S_i
Common values	5	50	65	45	427	30.7	0.8723	
Optimal values	8	60	40	45	287	22.1	1.4502	1.236
Improvements / %					–32.8	–28.0	66.3	

Table 9 Experimental confirmation

Method	*I* (A)	*V* (V)	*O* (µs)	*F* (µs)	*DH*(µm)	*TP*(x10⁻³)	*MRR*(mm³/s)
Optimization	8	60	40	45	287	22.1	1.4502
Experiment	8	60	40	45	284	21.8	1.4302
Errors (%)					1.05	1.36	1.38

Table 6 Computed ANOVA results for the *MRR*

So.	SS	MS	F value	p-value
Model	2.73	0.195	48.735	< 0.0001
I	0.650	0.650	162.500	< 0.0001
V	0.630	0.630	157.500	< 0.0001
O	0.610	0.610	152.500	< 0.0001
F	0.340	0.340	85.000	< 0.0001
IV	0.017	0.017	4.250	0.0781
IO	0.037	0.037	9.250	0.0004
IF	0.330	0.330	82.500	< 0.0001
VO	0.043	0.043	10.750	0.0002
VF	0.060	0.060	15.000	< 0.0001
OF	0.002	0.002	0.493	0.3085
I^2	0.000	0.000	0.115	0.6176
V^2	0.002	0.002	0.417	0.3475
O^2	0.016	0.016	4.000	0.0862
F^2	0.030	0.030	7.500	0.0011
Res.	0.061	0.004		
Cor.	2.790			
R^2: 0.9782; Adj. R^2: 0.9626; Pred. R^2: 0.9538				

Tab. 7 presents comparisons between the experimental and predictive values for the RBFN models. Low deviations (less than 5.0%) indicate that the proposed correlations are accurate.

4.2 Optimality

The MQPSO is applied to produce Pareto graphs (Fig. 9), in which the best optimality is selected with the highest

I_i value. The optimal values generated by the MQPSO of the *I*, *V*, *O*, and *F* are 8 A, 60 V, 40 µs, and 45 µs, respectively. The *DH* and *TP* are reduced by 32.8% and 22.1%, respectively, while the *MRR* is enhanced by 66.3% in comparison with common values (Tab. 8).

The experimental confirmation is executed at the optimal solution. The errors of the *DH*, *TP*, and *MRR* are 1.05%, 1.36%, and 1.38%, respectively, indicating the precision of the optimizing data.

4.3 Practical Contributions

The practical contributions are expressed as:

The impacts of EDDH inputs on the responses can be considered as effective knowledge for laborers.

The *DH*, *TP*, and *MRR* can be used to forecast the response values in the practical EDDH process.

The achieved data of this investigation can be utilized to develop an intelligent system for deployment of the EDDH operation in various industrial sectors.

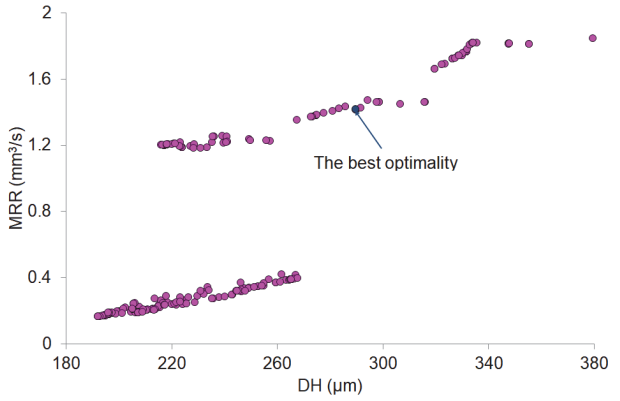

(a) *MRR* versus *DH*

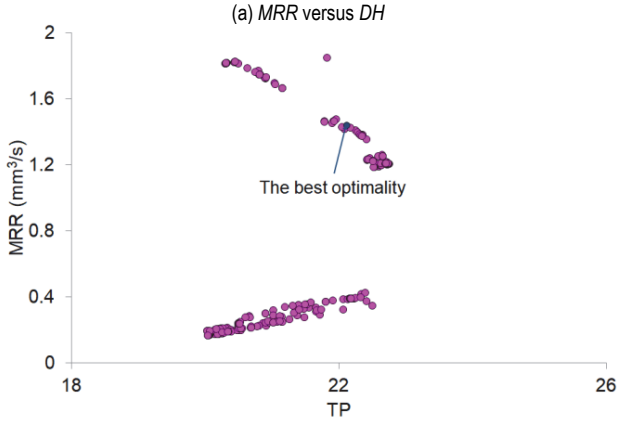

(b) *MRR* versus *TP*

Figure 9 Pareto fonts produced by the MQPSO

5 CONCLUSIONS

In order to reduce the *DH* as well as *TP* and increase the *MRR*, the best EDDH inputs (*I*, *V*, *O*, and *F*) were chosen for the current study. The MQPSO was employed to provide workable solutions, and the RBFN method was used to suggest EDDH replies. EAMR was applied in order to identify optimal results. The following is how the conclusions are presented:

1. It was suggested that the maximum *F* be employed, but the low *I*, *V*, and *O* should be used to reduce the *DH*. While the lowest values of the *I* and *O* were given, the greatest data from the *V* and *F* were used to lower the *TP*. The maximum parameters were used in order to optimize the *MRR*.

2. With the ranges of inputs, the *DH*, *TP*, and *MRR* changes from 286 to 476 µm, 22.2 to 36.9 × 10^{-3}, and 0.3698 to 1.6767 mm^3/s, respectively.

3. With the *DH* and *TP*, the *O* and *F* were found to be the most effective factors. With the *MRR*, the *I* and *V* were found to be the most significant parameters.

4. The optimal *I*, *V*, *O*, and *F* were 8 A, 60 V, 10 µs, and 45 µs, respectively. The *DH* and *TP* were reduced by 32.8% and 28.0%, respectively, while the *MRR* was enhanced by 66.3%.

6. Reducing the *DH* as well as *TP* and enhancing the *MRR* is practical approach, as compared to the single optimization.

7. The production cost and air pollution have not been analyzed. The impacts of process parameters on the production cost and air pollution can be considered in the next publications.

6 REFERENCES

[1] Kumar, A. & Pradhan, M. K. (2023). An ANFIS modelling and genetic algorithm-based optimization of through-hole electrical discharge drilling of Inconel-825 alloy. *Journal of Materials Research*, *38*, 312-327. https://doi.org/10.1557/s43578-022-00728-6

[2] Pandey, G. K. & Yadav, S. K. S. (2023). Experimental investigation to evaluate the effect of low frequency vibration on performance of vibration assisted electrical discharge drilling of titanium alloy. *International Journal on Interactive Design and Manufacturing*. https://doi.org/10.1007/s12008-023-01589-x

[3] Davis, R. et al. (2022). Effect of tool geometry on the machining characteristics amid sic powder mixed electric discharge drilling of hybrid metal matrix composite. *Silicon*, *14*, 27-45. https://doi.org/10.1007/s12633-020-00763-0

[4] Naik, S., Das, S. R., & Dhupal, D. (2021). Experimental investigation, predictive modeling, parametric optimization and cost analysis in electrical discharge machining of Al-SiC metal matrix composite. *Silicon*, *13*, 1017-1040. https://doi.org/10.1007/s12633-020-00482-6

[5] Kumar, N. et al. (2023). Investigation and optimization in electrochemical arc drilling of Ni55.7Ti nickel-titanium shape memory alloy with molybdenum electrode. *Journal of the Brazilian Society of Mechanical Sciences and Engineering*, *45*, 448. https://doi.org/10.1007/s40430-023-04374-9

[6] Gao, C. et al. (2021). Influence of electrical discharge machining on thermal barrier coating in a two-step drilling of nickel-based superalloy. *Arabian Journal for Science and Engineering*, *46*, 2009-2020. https://doi.org/10.1007/s13369-020-04987-5

[7] Kar, S. et al. (2021). Parametric optimization of µEDM drilling on titanium using principal component analysis. *Journal of the Brazilian Society of Mechanical Sciences and Engineering*, 43, 543. https://doi.org/10.1007/s40430-021-03249-1

[8] Saxena, R. et al. (2022). Experimental investigation of electrochemical discharge drilling (ECDM-D) performance characteristics for N-BK7 glass material. *International Journal on Interactive Design and Manufacturing*. https://doi.org/10.1007/s12008-022-01057-y

[9] Gajjal, P. & Dahake, M. R. (2023). A novel optimized dielectric fluid electric discharge machine using African

buffalo optimization. *International Journal on Interactive Design and Manufacturing*.
https://doi.org/10.1007/s12008-023-01591-3

[10] Desai, D. J. K., Singh, A. K., Sharma, A. et al. (2023). Experimental investigation & optimization of micro-hardness and surface roughness under electric discharge machining: to enhance superalloy Superfer 800 lightweight industrial applications. *International Journal on Interactive Design and Manufacturing*.
https://doi.org/10.1007/s12008-023-01581-5

[11] Ammisetti, D. K. & Kruthiventi, S. S. H. (2023). Experimental analysis and artificial neural network teaching-learning-based optimization modeling on electrical discharge machining characteristics of AZ91 composites. *Journal of Materials Engineering and Performance*.
https://doi.org/10.1007/s11665-023-08795-4

[12] Gunasekar, D. et al. (2023). Performance analysis of different dielectric on electrical discharge machined AA8011/SiC/Si3N4 composites using Taguchi coupled ELECTRE approach. *Silicon*.
https://doi.org/10.1007/s12633-023-02696-w

[13] Pratap, S. et al. (2023). An analysis to enhance the machining performance of micro-EDM for drilling of blind micro-hole using ANN. *International Journal of Advanced Manufacturing Technology*, 129, 2551-2561.
https://doi.org/10.1007/s00170-023-12476-w

[14] Pandey, G. K. & Yadav, S. K. S. (2022). Experimental investigation of vibration assisted electrical discharge drilling of Al-Tib2. *International Journal on Interactive Design and Manufacturing*.
https://doi.org/10.1007/s12008-022-01002-z

[15] Manivannan, R. & Pradeep Kumar, M. (2018). Improving the machining performance characteristics of the µEDM drilling process by the online cryogenic cooling approach. *Materials and Manufacturing Processes*, *33*(4), 390-396.
https://doi.org/10.1080/10426914.2017.1303145

[16] Chen, K. et al. (2022). Design and experiment of a wheel precision seed-metering device with cells for corn. *Tehnički vjesnik*, *29*(5), 1741-1748.
https://doi.org/10.17559/TV-20211126025302

[17] Gai, S. et al. (2023). Optimization of forged 42CrMo4 steel piston pin hole profile using finite element method. *Tehnički vjesnik*, *30*(1), 80-86.
https://doi.org/10.17559/TV-20220330131907

[18] Qin, B., Fan, Y., & Gao, Y. (2022). Distributed adaptive control for a class of heterogeneous nonlinear multi-agent systems with nonidentical dimensions. *Tehnički vjesnik*, *29*(5), 1537-1544. https://doi.org/10.17559/TV-20220417095645

Contact information:

An-Le VAN
Robotics and Mechatronics Research Group,
Faculty of Engineering and Technology,
Nguyen Tat Thanh University,
300A Nguyen Tat Thanh Street, Ward 13, District 4,
Ho Chi Minh City 70000, Vietnam
E-mail: lvan@ntt.edu.vn

Trung-Thanh NGUYEN
Faculty of Mechanical Engineering,
Le Quy Don Technical University,
236 Hoang Quoc Viet, Ha Noi 100000, Vietnam
E-mail: trungthanhnguyen@lqdtu.edu.vn

Phan Nguyen HUU
Hanoi University of Industry,
No. 298, Cau Dien Street, Bac Tu Liem District,
Ha Noi 100000, Vietnam
E-mail: nguyenhuuphan@haui.edu.vn

Xuan-Ba DANG
(Corresponding author)
Department of Automatic Control,
Ho Chi Minh City University of Technology and Education,
No. 1 Vo Van Ngan Street, Linh Chieu Ward, Thu Duc City,
Ho Chi Minh City 70000, Vietnam
E-mail: badx@hcmute.edu.vn